JOURNAL OF SPACECRAFT AND ROCKETS
Vol. 34, No. 6, November–December 1997

Control Effectiveness of a Jet–Slender Body Combination at Hypersonic Speeds

K. Kontis* and J. L. Stollery†
Cranfield University, Bedfordshire MK43 0AL, England, United Kingdom

The effects of jet control on the aerodynamic characteristics, performance, and stability of a 5-deg semiangle slender cone missile configuration are studied. Tests were made in the Cranfield University College of Aeronautics hypersonic gun tunnel using both sharp and blunted cones. The study was conducted at a Mach number of 8.2 and a Reynolds number of 392,700, based on base diameter, at pitch angles of −15 to 15 deg. The boundary layer was laminar. Air was used as the working gas for both the freestream and the sonic jet. The tests employed schlieren photography to study the overall flowfield. Quantitative studies of the effect of the jet have been made by pressure measurements. The forces were measured with a three-component balance equipped with semiconductor strain gauges.

Nomenclature

A = area
C = Chapman–Rubesin constant
C_A = axial force coefficient
Cd = nose drag coefficient
C_m = pitching moment coefficient
C_N = normal force coefficient
d = diameter
$F_{j,v}$ = measured jet force without any external flow, i.e., M_∞ is 0
h = penetration height
K = amplification factor
L = total cone length
L_{sep} = separation distance
L_0 = measured aerodynamic force with jet off
L_1 = measured total aerodynamic force with jet on
M = Mach number
P = pressure
T = temperature
x = distance from the nose
x' = distance along the jet meridian from jet nozzle
α = angle of attack, deg
γ = ratio of specific heats
δ = cone semiangle
δ_e = equivalent half-cone angle
ε = $(\gamma - 1)/(\gamma + 1)$
κ_ε = bluntness parameter, $M^3 Cd\varepsilon(d_n/x)$
Φ = ray angle of sharp cone
φ = flow momentum flux
χ = viscous interaction parameter, $M^3\sqrt{(C/Re_x)}$
χ_ε = $\varepsilon[0.664 + 1.73(T_w/T_o)]\chi$

Subscripts

b = base
e = jet exit
j = jet flow property
n = nose
w = wall
o = total value
1 = condition behind a shock
2 = condition ahead separation
∞ = freestream

Presented as Paper 96-2470 at the AIAA 14th Applied Aerodynamics Conference, New Orleans, LA, June 17–20, 1996; received Aug. 29, 1996; revision received July 10, 1997; accepted for publication July 15, 1997.

*Ph.D. Student/Research Assistant, Flow Prediction and Control Group, College of Aeronautics.

†Professor Emeritus of Aerodynamics, Flow Prediction and Control Group, College of Aeronautics. Fellow AIAA.

Introduction

IN situations where conventional aerodynamic surfaces cannot function properly, due either to the low density of the medium or to the considerable aerodynamic heating effects, secondary fluid injection is proposed as an attractive method of controlling the flight path. Even in cases where the interaction force becomes very small, as in rarefied flows, the jet thrust is still available for control. The complexity of flowfields created by jets interacting with external flows is such that the present understanding of them relies heavily on experimental data.[1–4]

The introduction of bluntness modifies the aerodynamic properties of the flow over a slender body from that with an equivalent sharp nose. The bow shock wave stands off from the nose and is highly curved, which give rise to gradients in flow properties normal to the cone surface. The stream tubes crossing the shock near the nose suffer a large entropy rise and then expand rapidly downstream. This entropy layer is a region of high temperature and low density, with total pressure losses due to the bow shock and lower local Mach number and unit Reynolds number than in the freestream. The entropy layer influences the local flow conditions for a large distance downstream, and eventually it is swallowed by the boundary layer. Simpkins[5] found that the introduction of nose bluntness promotes separation. He did an experimental comparison of the interaction between a radial underexpanded jet and the hypersonic flow over a sharp and a blunt cone of semiangle 5 deg at a freestream Mach number of 13, with laminar boundary layers. Kumar[6] identified some of the parameters that determine the upstream extent and lateral spreading of the separation front around an underexpanded transverse jet on a slender blunted cone, under laminar conditions. Holden[7] showed that, under entirely laminar conditions, the extent of the separated region was related to the viscous bluntness interaction parameter, $(\chi_\varepsilon \kappa_\varepsilon^{2/3} \sim M/[d_n^{2/3}\sqrt{Re_x}])$, which takes into account the relative effects of changes in Mach and Reynolds numbers on the extent of the interaction. For $0.1 \le \chi_\varepsilon \kappa_\varepsilon^{2/3} \le 0.5$ (small bluntness), the introduction of leading-edge bluntness promoted separation, whereas for $\chi_\varepsilon \kappa_\varepsilon^{2/3} \le 0.1$ (large bluntness), the leading-edge bluntness resulted in a reduction in the extent of boundary-layer separation.

Experimental Setup

The experiments were conducted in the College of Aeronautics gun tunnel, with air as the working jet and freestream gas, at $M_\infty = 8.2$. A description of the setup and calibration of the facility are given by Stollery et al.[8] and Needham.[9] The flow is uniform inside the test section except on the centerline,[10] where the Mach number varies by ±4.5%. Pressure measurements were carried out using Kulite XCS-190 absolute pressure transducers. The forces were measured with a three-component balance having an accuracy of normal force and pitching moment ±1.5% and of axial force ±2.5% (Ref. 10). A repeatability of 97%, of the force and moment coefficients, was achieved in the present investigation over six runs.

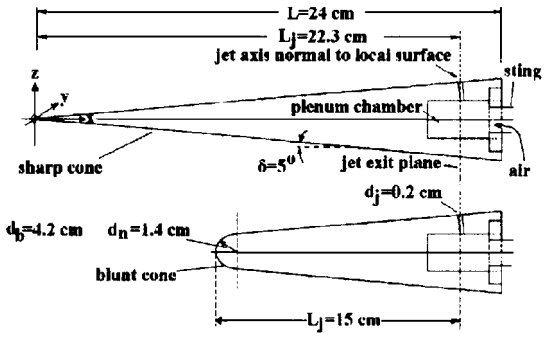

Fig. 1 General geometry of the models.

The general geometrical characteristics of the configurations are shown in Fig. 1. Both models have the same base diameter. For the blunt cone, the bluntness ratio was 33.3% ($d_n/d_b = \frac{1}{3}$). The models were equipped with a single jet hole. Pressure models were equipped with tappings along the jet meridian.

Analytical Models

Blunt Cone

$\alpha = 0$ Degree

For a blunt body, the boundary-layer stream tube is processed by the strong, near-normal section of the nose shock. The Rayleigh–pitot relationship[11] gives the reservoir pressure downstream of a normal shock. Assuming the flow at the edge of the boundary layer to be isentropic, then

$$M_2 = \sqrt{[2/(\gamma-1)]\left\{[(P_{o1}/P_\infty)(P_\infty/P_2)]^{(\gamma-1)/\gamma} - 1\right\}} \qquad (1)$$

$\alpha \neq 0$ Degree

Cheng et al.[12] have shown that the shock structure close to the axis of a blunt cone at incidence, $\alpha \neq 0$ deg, is determined by the shape of the nose. As with the zero incidence case, the surface stream tubes, on a blunt cone at incidence, are processed by a normal shock. The reservoir pressure within these stream tubes can be approximated to that immediately downstream of a normal shock. The Mach number on the blunt cone, at incidence, was determined by substituting from the Rayleigh–pitot relationship and the measured pressure P_2 into Eq. (1).

Sharp Cone

$\alpha = 0$ Degree

From Brower's tables,[13] the local surface Mach number was interpolated, $M_2 = 7.39$.

Windward Top Generator, $\alpha \geq \delta$

High and Blick[14] used the concept of the equivalent cone (a right circular cone at zero incidence having the same freestream Mach number and a half-cone angle equal to the angle between the freestream Mach number vector and the ray line on the cone under examination). Angle δ_e was calculated by

$$\delta_e = \sin^{-1}(\sin\delta\cos\alpha + \cos\delta\sin\alpha\cos\Phi) \qquad (2)$$

with $\Phi = 0$ deg along the bottom generator and 180 deg along the top generator. The local Mach number was calculated for δ_e evaluated at $\Phi = 180$ deg. For $\Psi < 1$,

$$M_2 = M_\infty \cos\delta_e \left(1 - \frac{\sin\delta_e}{M_\infty}\right)^{0.5} \times \left\{[1 + \exp(-1 - 1.52\Psi)]\left[1 + \left(\frac{\Psi}{2}\right)^2\right]\right\}^{-0.5} \qquad (3)$$

If $\Psi \geq 1$, where Ψ is the hypersonic similarity parameter, $M_\infty \sin\delta_e$,

$$M_2 = M_\infty \cos\delta_e \left(1 - \frac{\sin\delta_e}{M_\infty}\right)^{0.5} (1 + 0.35\Psi^{1.5})^{-0.5} \qquad (4)$$

Leeward Top Generator, $\alpha \geq \delta$

A Prandtl–Meyer expansion was assumed from the freestream conditions to the surface values and because the flow is isentropic:

$$M_2 = \sqrt{\frac{2}{\gamma-1}\left\{\frac{1 + [(\gamma-1)/2]M_\infty^2}{(P_2/P_\infty)^{(\gamma-1)/\gamma}} - 1\right\}} \qquad (5)$$

Results and Discussion

The jet flowfield interaction is shown in Fig. 2. The experiments were conducted with a sonic highly underexpanded jet ($P_{0j} = 110$ psia, $P_{oj}/P_\infty \approx 800$). Because of the relatively high Mach number and the low Reynolds number, in the absence of the jet, the initial boundary layer on the surface of the cones was laminar. The jet plume presents an obstacle to the external flow (Fig. 2), which causes a strong shock, which causes the boundary layer upstream of the jet to separate. In contrast to the two-dimensional situation in which the entire external flow must go over the jet-induced obstruction, the flow can go around the three-dimensional jet. The flowfield near the separation point is controlled by the interaction between the resultant free shear layer and the external stream. As a result of high pressures downstream of the separation shock and mixing between the two streams, the jet is turned in the direction of the external flow (Fig. 2). A three-dimensional shock structure forms in the jet plume as it is turned, bounded by a three-dimensional mixing layer. Some of the high-pressure external air behind this separation shock flows downstream, causing a high-pressure region in front of the jet. From this high-pressure region, the external air also flows radially outward along the surface of the cone, expanding to lower pressures. Finally, this expanding reverse flow is terminated by a shock system. As the reverse flow continues outward from the jet, it turns toward the downstream direction. To satisfy the boundary conditions, at least two counter-rotating vortices must be present within the upstream separated region (Fig. 2), the clockwise separation vortex in the separated flow region and the counterclockwise jet horseshoe vortex in the region immediately upstream of the jet. An important feature of interest is the strong shock, which terminates the supersonic region of the jet (often referred to as the Mach disk or normal shock). The Mach disk is dish shaped and parallel to the exit plane (Fig. 2). Figures 3 and 4 show the absence of a separation shock wave along the 180-deg meridian, which means that the flow remains attached along this meridian and, hence, the shape of the separated region must be similar to Fig. 2.

Parameters for Data Presentation

The ratio of jet to undisturbed flow momentum flux[15] was used as the control parameter of the problem with $d_b = 4.2$ cm, $d_j = 0.2$ cm, $\gamma_j = \gamma$, $M_j = 1$, and $P_{oj}/P_j = 1.892$:

$$\frac{\varphi_j}{\varphi_\infty} = \frac{\rho_j u_j^2 A_j}{\rho u_\infty^2 A_b} = \frac{P_j \gamma_j M_j^2 A_j}{P_\infty \gamma M_\infty^2 A_b} \sim \frac{P_j d_j^2}{P_\infty M_\infty^2 d_b^2} \sim \frac{P_{oj}}{P_2 M_2^2} \qquad (6)$$

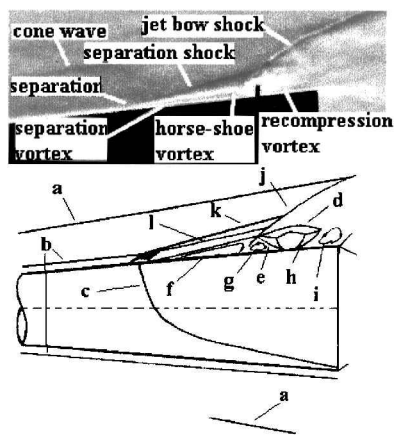

Fig. 2 General structure of the interaction region for the sharp cone at $\alpha = 0$ deg: a, cone shock; b, boundary layer; c, separation front; d, Mach disk; e, jet boundary; f, separation vortex; g, horseshoe vortex; h, internal shocks; i, recompression vortex; j, jet bow shock; k, separation shock; and l, separated boundary layer.

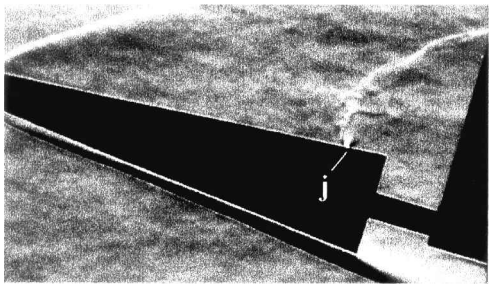

a) α = 15 deg

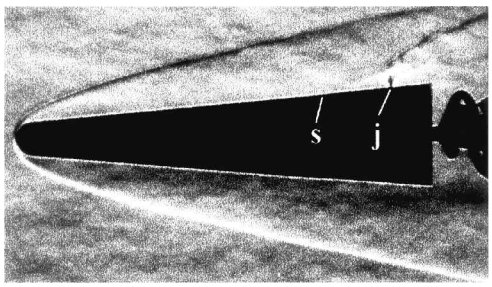

d) α = 0 deg

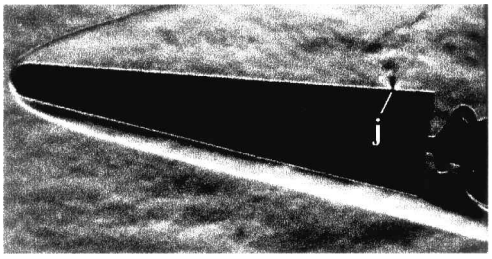

b) α = 10 deg

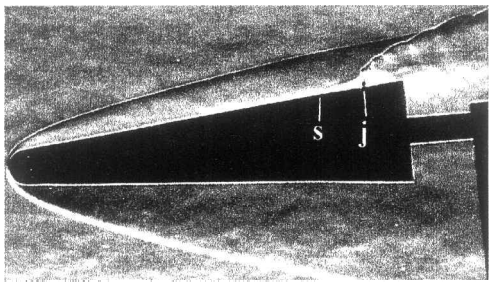

e) α = −5 deg

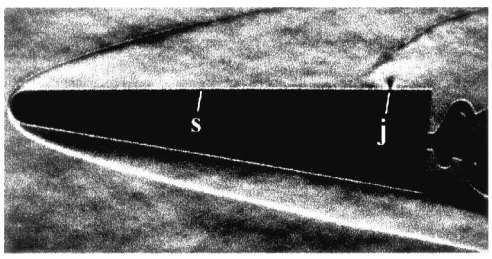

c) α = 5 deg

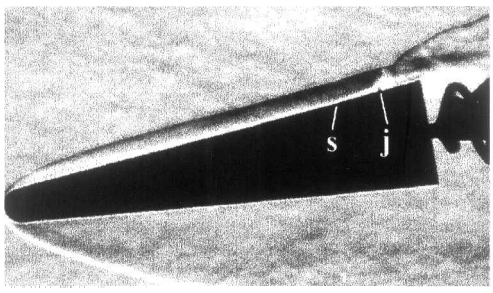

f) α = −10 deg

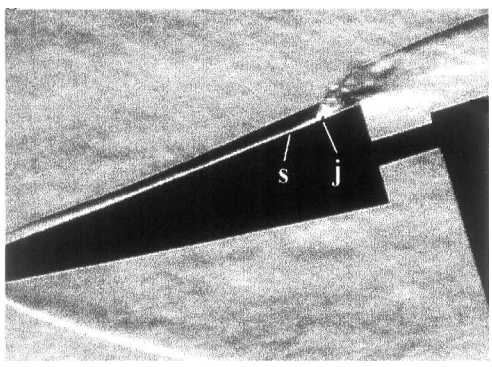

g) α = −15 deg

Fig. 3 Schlieren visualization studies for the blunt cone.

The interaction force due to the pressure distribution induced on the body by the interaction between the jet and the cone flow can be represented in the form of amplification factor:

$$K = \frac{L_1}{L_0 + F_{j,v}} \tag{7}$$

Effect of Bluntness

Figures 3 and 4 show that the introduction of nose bluntness, although it effectively increases the jet by reducing the local surface pressure ahead of the separation region, causes a delay in separation. The nose bluntness causes the boundary layer to grow by mutual interaction with the entropy layer and increases the magnitude of the favorable pressure gradient upstream of the jet and, consequently, causes the velocity distribution in the boundary layer to be fuller close to the body. The reduced lengths of the separated regions are also evident from the pressure distributions (Fig. 5). Substituting $d_n/x = 0.0936$ (corresponding to the location of jet orifice), $Cd = 0.964$, $M_\infty = 8.2$, $T_w = 296$ K, $T_o = 1290$ K, $\gamma_\infty = 1.4$, $C \approx 1$, and $Re_x = 1.349 \times 10^6$ into Holden's[7] equations (given in the Introduction), it was found that $\chi_\varepsilon \kappa_\varepsilon^{2/3} = 0.0387$, which is lower than 0.1. Thus, Holden theory also predicted the reduction of separation, at 0-deg incidence for the blunt cone, compared to the equivalent sharp cone, although his theory is based on experiments on flat plates. From Stetson's data[16] the distance needed for the boundary layer to swallow the entropy layer was calculated as 2 m, which means that for the blunt model ($L = 16.7$ cm) the whole flowfield around the cone is influenced by the entropy layer. The boundary-layer edge becomes totally invisible for the blunt cone (Figs. 3a and 3b). This is because the highly curved shock wave produces

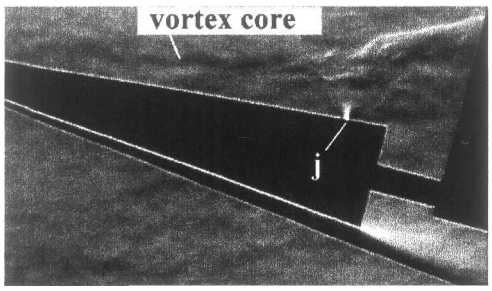

a) α = 15 deg

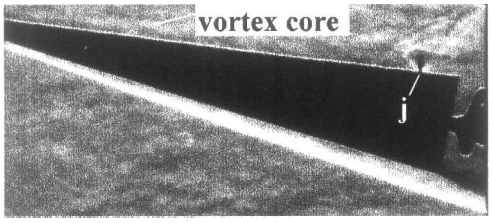

b) α = 10 deg

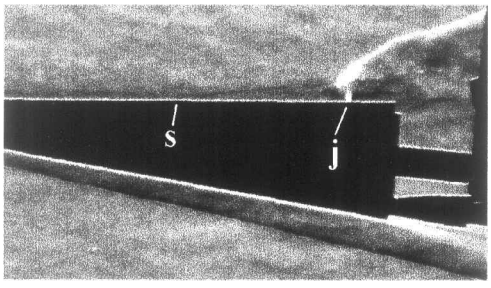

c) α = 5 deg

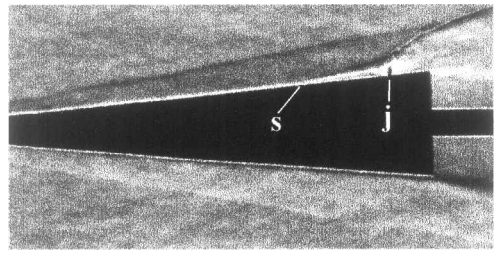

d) α = 0 deg

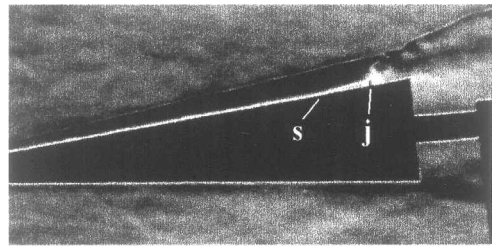

e) α = −5 deg

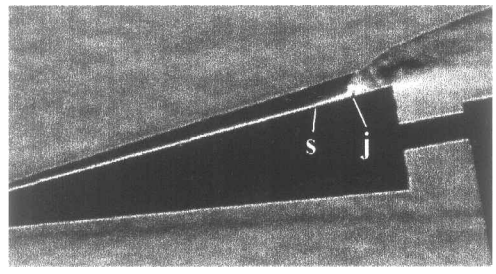

f) α = −10 deg

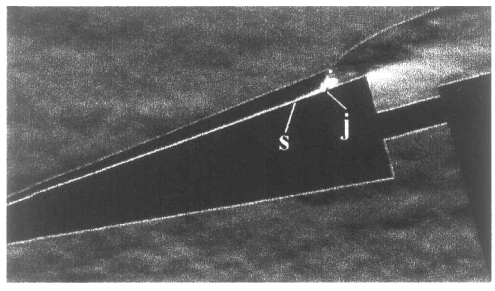

g) α = −15 deg

Fig. 4 Schlieren visualization studies for the sharp cone.

strong density gradients throughout the entire flowfield that obscure the density gradients in the boundary layer, thus making the identification of separation of the flow very difficult.

The pressure measurements at zero incidence without jet (Fig. 6) show that the effect of the nose bluntness is felt over the entire body length. The surface pressure distribution is reduced by the expansion at the shoulder to about 70% of the sharp cone values. Because of the lower undisturbed surface pressure on the blunt cone (Fig. 5), the jet pressure ratio P_{oj}/P_2 is higher on the blunt cone than on the sharp cone and, therefore, the jet penetration into the undisturbed flow will be greater in the blunt cone case, e.g., Figs. 3a and 4a. The difference between the two cones reduces as incidence decreases (Figs. 3 and 4). This is because the bluntness effect on surface pressure distribution diminishes and approaches the equivalent sharp cone surface pressure near the jet as the angle of attack decreases (Fig. 6). The jet bow shock is closer to the jet for the sharp configuration, e.g., Figs. 3d and 4d; this is due to the higher total pressure in the shock layer and the higher local stream velocity (as the local surface Mach number is higher than for the blunt cone case). An oscillation of the bow wave ahead of the jet is apparent in all of the figures and indicates the unsteady nature of the jet interaction with the separated shear layer.

Effect of Incidence

The effect of incidence is to decrease the local Mach number and increase the local Reynolds number along the windward ray. On the leeward ray, the local Mach number increases, and the local Reynolds number decreases. For the attached crossflow case ($\alpha \leq \delta$), Figs. 3c, 3e, 4c, and 4e show a thickening of the boundary layer along the leeward meridian. A decrease in heat transfer along the leeward meridian is expected,[6] and it is due to the decrease in pressure in the leeward region of the cones (Fig. 6). Figure 6 shows a progressive decrease in cone pressure along the leeward meridian with incidence. The decrease in the local cone pressure along the leeward meridian with incidence effectively increases the local jet pressure ratio P_{oj}/P_2. The increased jet pressure ratio increases the diameter and penetration of the jet, which strengthens the interaction, promotes separation along the leeward meridian, and increases the

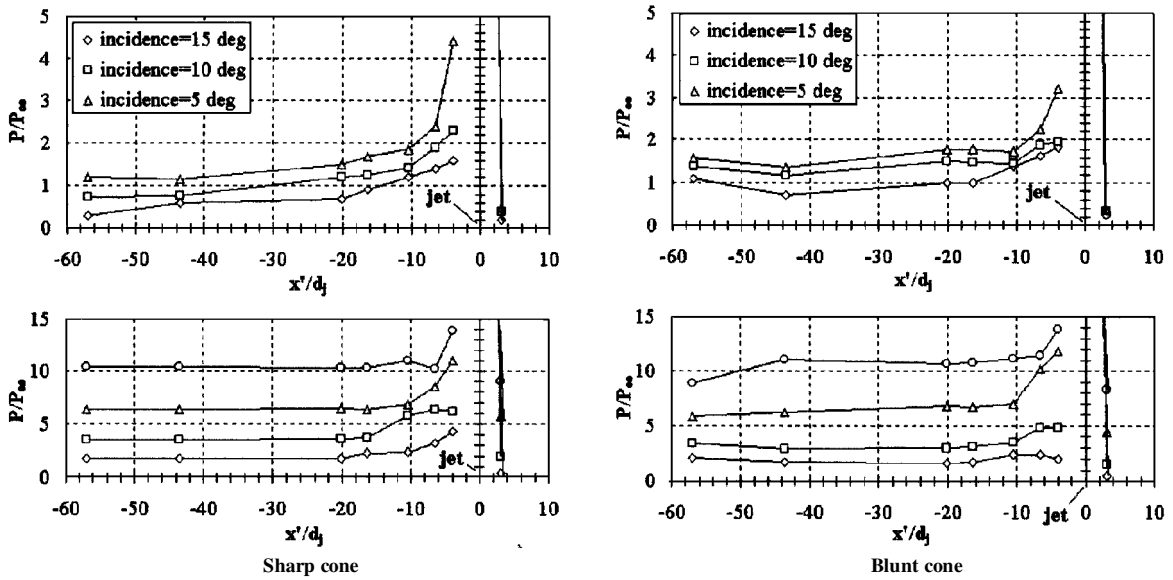

Fig. 5 Pressure distributions in the interaction region, along the jet meridian. Bottom panels: ◇, incidence = 0 deg; □, incidence = −5 deg; △, incidence = −10 deg; and ○, incidence = −15 deg.

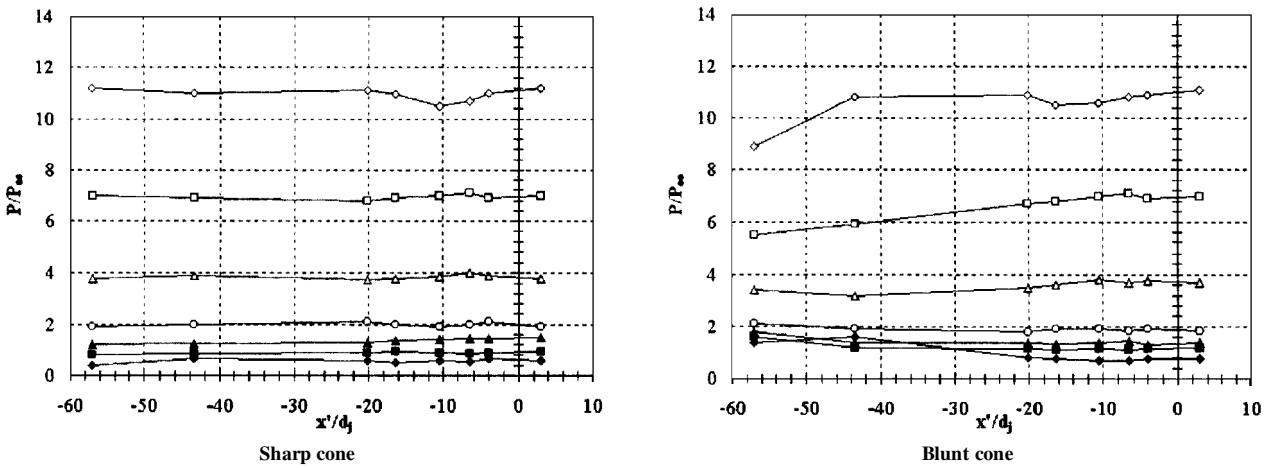

Fig. 6 Pressure distributions without jet: ◇, incidence = −15 deg; □, incidence = −10 deg; △, incidence = −5 deg; ○, incidence = 0 deg; ▲, incidence = 5 deg; ■, incidence = 10 deg; and ♦, incidence = 15 deg.

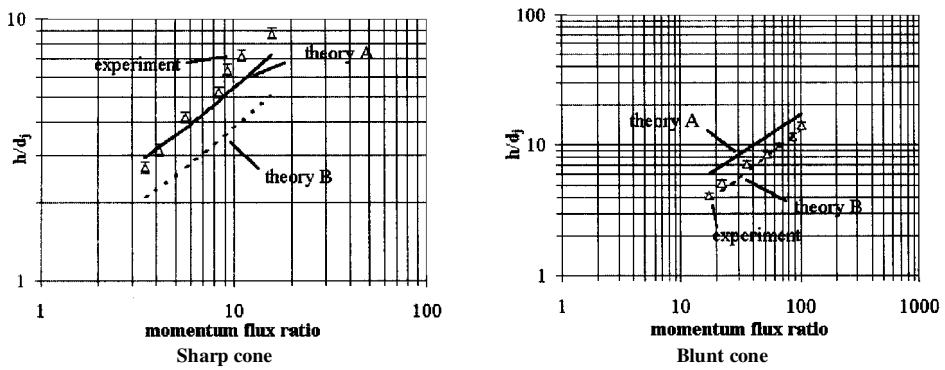

Fig. 7 Correlation of jet penetration heights.

jet bow shock standoff distance (Figs. 3 and 4) and the diameter of the jet horseshoe vortex.[6]

For the separated crossflow case ($\alpha > \delta$), Figs. 3a, 3b, 3f, 3g, 4a, 4b, 4f, and 4g show the establishment of a disturbed flow region over the leeward surface. This is probably due to separation of the crossflow, resulting in the establishment of a pair of counter-rotating vortices, over the leeward region of the body. At these incidences, the leeward jet exhausts into a complex separated crossflow structure. The density gradients associated with the crossflow vortices mask the gradients associated with the jet interaction region and, thus, make it difficult to observe the effects of the jet on the local flowfield. Figures 4a and 4b, on the leeward side, seem to show an increase in the strength of the crossflow vortices as the incidence increases, which agrees with results on experiments on a tangent ogive/cylinder configuration[17] and on an elliptic cone configuration.[18]

Equivalent Penetration Model

The schlieren pictures of the shock patterns produced by the jet injection are reminiscent of the flow around a cylinder protruding from a solid surface. Based on this analogy, the modified equation of Zukoski and Spaid[19] was used, where the pressure coefficient corresponds to the stagnation pressure of the equivalent cylinder protruding behind a normal shock in the primary flow of Mach number M_2. Theory A of Ref. 19 assumes that the jet interaction resembles that of a quarter-sphere–half-cylinder model, whereas theory B of Ref. 19 assumes that of a spherical nosed cylinder. Figure 7 shows that theory B seems to agree better with the experimental findings of the blunt cone, whereas theory A seems to agree better with the experimental findings of the sharp cone. This is some indication of the different shape of disturbance.

Pressure Measurements

The distributions in the interaction region show a repeatability of ±5%. Separation was taken to be at the midpoint between the cone pressure and the plateau pressure levels. The location correlates well with schlieren observations of the location of the separation shock. Figures 5 and 6 show that the resulting separation alters the surface pressure distribution ahead of the jet. The separated flow region behind the jet makes a negative contribution to the control force, inasmuch as near the base of the models the surface pressure was found to be consistently lower than the undisturbed cone values (Fig. 5) as the primary flow expands around the jet. The separated flow ahead of the jet makes a positive contribution to the control force, and this is the more significant effect resulting in amplification factors greater than unity.

The pressure along the jet meridian increases on the surface of the cones to the point at which flow separates, and then there is a further rise to a pressure plateau. In the vicinity of the jet, the pressure distribution shows a small drop from the plateau value. After this drop, the pressure rises to a peak just ahead of the jet. The position of this peak corresponds with the location of the main reattachment ahead of the jet. A correlation of the length of the separated flow along the jet meridian for the two cone configurations is shown in Fig. 8. The correlation suggests that the length of the separated flow region increases with an increase in the jet to undisturbed flow surface value pressure ratio and a decrease in the local Mach number ahead the separation. The range of variables was limited and more data are required.

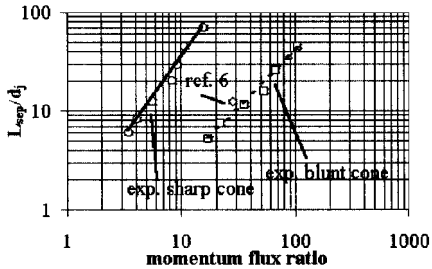

Fig. 8 Correlation of the separated flow length along the jet meridian.

Force Measurements

The calculated force and moment values were nondimensionalized using the base area and base diameter as reference values. The pitching moment was measured at the moment reference point located at $x'/d_j = -10.2$ along the body axis measured from the jet nozzle. The effects of the jet interaction were studied by establishing

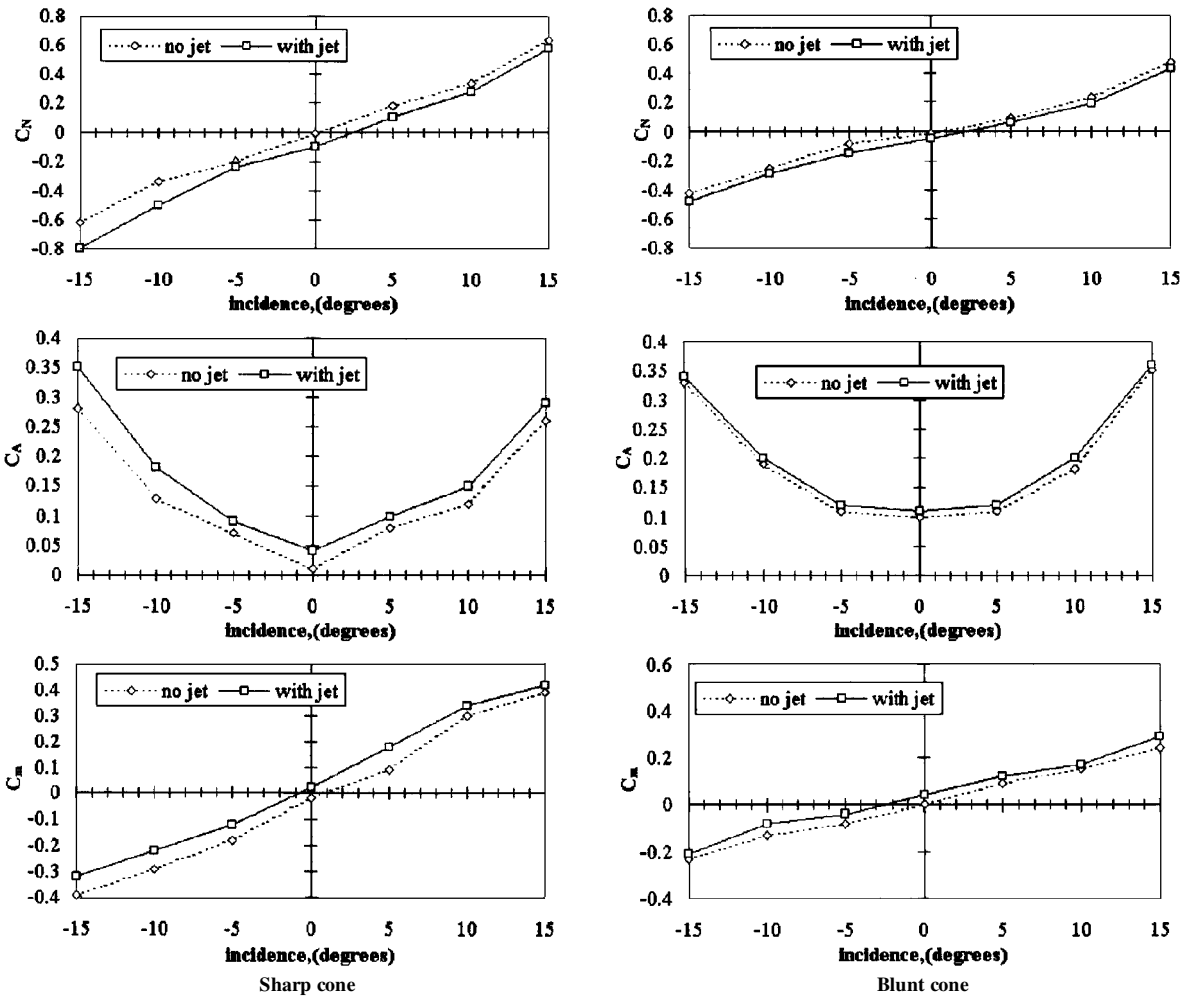

Fig. 9 Effect of jet and jet interaction on the aerodynamics coefficients.

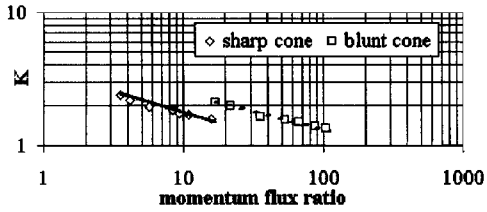

Fig. 10 Correlation of amplification factor.

a steady jet and then firing the tunnel. The presence of the jet at $t = 0$ ms produces a negative force. The magnitude of this force is constant after 100 ms because of the jet plenum chamber becoming choked. The firing of the tunnel initiates the aerodynamic forces, and the increase in pressure in the interaction region augments the jet force. The completion of the tunnel run and the consequent removal of the augmentation force results in the force measured returning to the jet force level.

Experimentally, under near vacuum conditions without the tunnel running, the jet-only contributions are a negative (downward) normal force $C_{N(j)} = -0.021$, a positive (backward) axial force $C_{A(j)} = 0.0042$, and a positive (nose-up) pitching moment (due to the jet axis being aft of the moment center) $C_{m(j)} = 0.0048$. Assuming an isentropic process to take place inside the jet nozzle, the theoretical jet-only contributions are[15] $C_{N(j)} = -0.035$, $C_{A(j)} = 0.0063$, and $C_{m(j)} = 0.008$. The theory overpredicts the jet-only contributions because in reality there are total pressure losses due to friction in the delivery tubing.

The aerodynamic coefficients measured on the cones, with and without jet, are shown in Fig. 9. The effect of the jet on the axial force coefficient is very small at all incidences. The effect of the jet is more pronounced on the normal force coefficient. The total induced force contributes a decrease at every incidence. The effect is to shift the normal coefficient curves to the right. This shift is of the same order, and each curve crosses the X axis at approximately 2.5-deg incidence. At $\alpha = 0$ deg, a small normal force $C_{N(\text{Blunt Cone})} = -0.011$ and a pitching moment $C_{m(\text{Blunt Cone})} = 0.004$ were measured on the blunt cone (in the absence of the jet), and a small normal force $C_{N(\text{Sharp Cone})} = -0.019$ and a pitching moment $C_{m(\text{Sharp Cone})} = -0.0015$ were measured on the sharp cone (in the absence of the jet). The forces and moments measured at 0-deg incidence, without the jet, are due to the centerline focusing effect associated with imperfections in the surface of the Mach 8.2 nozzle. At $\alpha = 0$ deg, the total normal force measured in the presence of the jet was $C_{N(\text{Blunt Total})} = -0.043$ for the blunt cone and $C_{N(\text{Sharp Total})} = -0.055$ for the sharp cone (including the normal force on the cones). For the blunt cone, the combined jet/interaction normal force was -0.032 ($C_{N(\text{Blunt Total})} - C_{N(\text{Blunt Cone})}$). This compares with the jet-only force of $C_{N(j)} = -0.021$. Thus, the interaction augments the total force generated by the jet by 52%. For the sharp cone, the combined jet and interaction normal force was -0.036 ($C_{N(\text{Sharp Total})} - C_{N(\text{Sharp Cone})}$). This compares with the jet-only force of $C_{N(j)} = -0.021$. Thus, the interaction augments the total force generated by the jet by 72%. The jet increases the moment on the cones (at $\alpha = 0$ deg) from $C_{m(\text{Blunt Cone})} = 0.004$ (in the absence of the jet) to $C_{m(\text{Blunt Total})} = 0.012$ for the blunt cone and from $C_{m(\text{Sharp Cone})} = -0.0015$ (in the absence of the jet) to $C_{m(\text{Sharp Total})} = 0.0075$ for the sharp cone. Therefore, the combined jet/interaction pitching moment for the blunt configuration is 0.008 ($C_{m(\text{Blunt Total})} - C_{m(\text{Blunt Cone})}$). This compares with the jet-only moment of $C_{m(j)} = 0.0048$. Thus, the interaction augments the pitching moment generated by the jet by 66%. For the sharp cone, the combined jet/interaction pitching moment is 0.009 ($C_{m(\text{Sharp Total})} - C_{m(\text{Sharp Cone})}$). This compares with the jet-only moment of $C_{m(j)} = 0.0048$. Thus, the interaction augments the pitching moment generated by the jet by 87.5%.

At $\alpha > 0$ deg, nose up, the jet causes the center of pressure to move forward. The main contribution toward the normal force and pitching moment comes from the region ahead the jet. At $\alpha < 0$ deg, nose down, the jet causes the center of pressure to move rearward. The main contribution toward the normal force and pitching moment comes from the vicinity of the jet and the region behind it. The amplification factor correlates well with the momentum flux ratio (Fig. 10). Smaller amplification factors were deduced for the blunt cone. This is because the size of the separated region is reduced. Augmentation factors of between 50 and 160% were deduced from the measurements (Fig. 10). The accuracy of the data given in Fig. 10 is connected to the balance accuracy and data manipulation. The maximum error is of the order $\pm 5\%$.

Conclusions

1) Nose bluntness causes a delay in separation with respect to the equivalent sharp cone configuration.

2) The penetration height increases on the leeward side and decreases on the windward side as incidence is increased.

3) The jet penetration is less for the sharp cone.

4) The momentum flux ratio is an important control parameter.

5) The interaction between the jet and the external flow causes a change in surface pressure around the injector. This pressure distribution modification results in a force that is about 50–160% larger than the nominal jet thrust.

6) The effect of the jet on the axial force coefficient is small.

7) The presence of the jet causes a rearward motion of the axial center of pressure at negative incidences and a forward motion at positive incidences.

References

[1]Spaid, F. W., and Cassel, L. A., "Aerodynamic Interference Induced by Reaction Controls," AGARD AG-173, Dec. 1973.

[2]Peake, D., and Tobak, M., "Three-Dimensional Interaction and Vortical Flows with Emphasis on High Speeds," AGARD AG-252, July 1980.

[3]Settles, G. S., and Dolling, D. S., "Swept Shock-Wave/Boundary-Layer Interactions," *Tactical Missile Aerodynamics: General Topics*, edited by M. J. Hemsch, Vol. 141, Progress in Astronautics and Aeronautics, AIAA, Washington, DC, 1992, pp. 505–574.

[4]Powrie, H. E. G., Ball, G. J., and East, R. A., "Experimental Study of the Interaction of a Two Dimensional Reaction Control Jet with a Hypersonic Flow," *Aerothermochemistry of Spacecraft and Associated Hypersonic Flows, Proceedings of the IUTAM Symposium/Marseilles* (France), International Union of Theoretical and Applied Mechanics, 1992, pp. 362–367.

[5]Simpkins, P., "Hypersonic Interactions About a Slender Cone Induced by Radial Mass Injection," *Hypersonic Boundary Layers and Flow Fields*, AGARD CP-30, 1968.

[6]Kumar, D., "Hypersonic Control Effectiveness," Ph.D. Thesis, Dept. of Aerospace Sciences, Cranfield Univ., Bedfordshire, England, UK, Jan. 1995.

[7]Holden, M. S., "Experimental Studies of Shockwave-Boundary Layer Interaction," AGARD AG-203, Jan. 1974.

[8]Stollery, J. L., Maull, D., and Belcher, B., "The Imperial College Hypersonic Gun Tunnel," *Journal of the Royal Aeronautical Society*, Vol. 64, Jan. 1959, pp. 24–30.

[9]Needham, D. A., "Progress Report on the Imperial College Hypersonic Gun Tunnel," Aeronautics Dept., TN 118, Imperial College of Science and Technology, London, Aug. 1963.

[10]Opatowski, T., "A Three Component Gun Tunnel Balance Designed for Testing Thin Delta Wings," Aeronautical Research Council, ARC 31 278, London, June 1969.

[11]"Equations, Tables and Charts for Compressible Flows," NACA Rept. 1135, Jan. 1953.

[12]Cheng, H. K., Hall, J. G., Golian, T. C., and Hertzberg, A., "Boundary Layer Displacement and Leading Edge Bluntness Effects in High Temperature Hypersonic Flow," *Journal of the Aerospace Sciences*, Vol. 28, No. 5, 1961, pp. 353–381.

[13]Brower, W. B., *Theory, Tables and Data for Compressible Flow*, Hemisphere, New York, 1990, pp. 65–70.

[14]High, W., and Blick, E., "Cone Pressure Distribution at Large and Small Angles of Attack," *AIAA Journal*, Vol. 2, No. 11, 1964, pp. 2054, 2055.

[15]Kontis, K., "Control by Blowing at Hypersonic Speeds," M.S. Thesis, Dept. of Aerospace Sciences, Cranfield Univ., Bedfordshire, England, UK, Aug. 1994.

[16]Stetson, K. F., "Effect of Bluntness and Angle of Attack on Boundary Layer Transition on Cones and Biconic Configurations," AIAA Paper 79-0269, Jan. 1979.

[17]Pagan, D., Molton, P., and Delery, J., "Basic Experiments on a Supersonic Vortex Flow Around a Missile Body," *Journal of Spacecraft and Rockets*, Vol. 29, No. 3, 1992, pp. 373–378.

[18]Kontis, K., Stollery, J. L., and Edwards, J. A., "Hypersonic Effectiveness of Slender Lifting Elliptic Cones With and Without Strakes," AIAA Paper 97-0521, Jan. 1997.

[19]Zukoski, E., and Spaid, F., "Secondary Injection of Gases into a Supersonic Flow," *AIAA Journal*, Vol. 2, No. 10, 1964, pp. 1689–1696.

R. M. Cummings
Associate Editor